

Article

# Cooling System Energy Consumption Reduction through a Novel All-Electric Powertrain Traction Module and Control Optimization

Simone Lombardi \*, Manfredi Villani \*, Daniele Chiappini  and Laura Tribioli 

Department of Industrial Engineering, University of Rome Niccolò Cusano, Via Don Carlo Gnocchi, 3, 00195 Rome, Italy; daniele.chiappini@unicusano.it (D.C.); laura.tribioli@unicusano.it (L.T.)

\* Correspondence: simone.lombardi@unicusano.it (S.L.); manfredi.villani@unicusano.it (M.V.)

**Abstract:** In this work, the problem of reducing the energy consumption of the cooling circuit for the propulsion system of an all-electric vehicle is approached with two different concepts: improvement of the powertrain efficiency and optimization of the control strategy. Improvement of the powertrain efficiency is obtained through a modular design, which consists of replacing the electric powertrain with several smaller traction modules whose powers sum up to the total power of the original powertrain. In this paper, it is shown how modularity, among other benefits, also allows reducing the energy consumption of the cooling system up to 54%. The energy consumption of the cooling system is associated with two components: the pump and the fan. They produce a so-called auxiliary load on the battery, reducing the maximum range of the vehicle. In conventional cooling systems, the pump and the fan are controlled with a thermostat, without taking into account the energy consumption. Conversely, in this work a control strategy to reduce the auxiliary loads is developed and compared with the conventional approach, showing that the energy consumption of the cooling system can be reduced up to 27%. To test the control strategy, numerical simulations have been carried out with a 1-D model of the cooling system. On the other hand, all the thermal loads of the components have been calculated with a vehicle simulator, which is able to predict the vehicle's behavior under different driving cycles.

**Keywords:** electric vehicle; propulsion cooling system; modularity; thermal management; control optimization



**Citation:** Lombardi, S.; Villani, M.; Chiappini, D.; Tribioli, L. Cooling System Energy Consumption Reduction through a Novel All-Electric Powertrain Traction Module and Control Optimization. *Energies* **2021**, *14*, 33. <https://doi.org/10.3390/en14010033>

Received: 15 November 2020

Accepted: 21 December 2020

Published: 23 December 2020

**Publisher's Note:** MDPI stays neutral with regard to jurisdictional claims in published maps and institutional affiliations.



**Copyright:** © 2020 by the authors. Licensee MDPI, Basel, Switzerland. This article is an open access article distributed under the terms and conditions of the Creative Commons Attribution (CC BY) license (<https://creativecommons.org/licenses/by/4.0/>).

## 1. Introduction

One of the most limiting factors of all-electric vehicles is the limited range [1,2]. The most advanced electric rechargeable energy storage systems (RESS), such as Li-ion batteries, still suffer of low energy density when compared to fuels, meaning that large and heavy batteries would be required to meet the travel range of conventional vehicles. In addition, severe ambient conditions can dramatically reduce the range and reliability of battery powered vehicles [3]. Another important drawback of all-electric vehicles is that the battery is the only energy storage on-board and therefore it is also required to provide the energy for the operation of the auxiliary loads, such as the air conditioning compressor and the fan and pump of the propulsion cooling system. In all-electric vehicles, reducing these loads is of primary importance, as they drain energy from the battery and can further decrease the range of the vehicle.

Generally, studies on the impact of auxiliary loads on energy consumption are limited to weather and climatic conditions—i.e., Heating, Ventilation, Air Conditioning (HVAC) consumption and thermal comfort measures [4–7]—driver behavior and traffic conditions. Lalhoul et al. [8] proposed a thermal comfort management approach that optimizes the thermal comfort while preserving the driving range during a trip is proposed. A large number of weather and traffic situations are simulated, and results show the efficiency

of the proposed approach in minimizing energy consumption while maintaining a good comfort. Similarly, Desreuveaux et al. [9], in order to plan the annual charging operation of an eco-campus, developed a simulation tool for an accurate determination of the consumption of an electric vehicle throughout the year. An overconsumption up to 33% in winter due to heating, and only 15% in summer due to air conditioning was found. Basciotti et al. [10] developed advanced simulation tools to improve the efficiency of climate control systems in order to accurately evaluate both the energy savings and thermal comfort.

On the other hand, very seldom the influence on energy consumption owe to cooling of powertrain components is included in the analysis. For example, the integrated thermal management of a pure electric vehicle is described in [11], including battery cooling/preheating, electric machines (EM) cooling and Air Conditioning (AC) or heat pump. Different approaches are proposed, but not modularity nor optimized control. Shojaei et al. [12] investigate the impact of the cooling power demands of the cabin and battery on the vehicle performance, focusing more on comfort levels and battery degradation. In [13], the National Renewable Energy Laboratory's modeling framework was used to explore control strategies for an electric vehicle combined loop system. The control approach included a mode selection algorithm and controllers for the compressor speed, cabin blower flow rate, coolant flow rate, and the front-end heat exchanger coolant bypass rate. The impact of these thermal systems on electric vehicle range during warmup was simulated showing up to a 10.9% improvement in range for the full system over the baseline during warmup from cold soak. The need to reduce the significant energy drain and resulting drive range loss due to auxiliary electrical loads is also addressed in [14].

As shown in the above literature review, in most of the research works, the problem of reducing the energy consumption of the auxiliary loads in an all-electric vehicle is translated into the effort of reducing the energy consumption of the AC system. On the other hand, in this work the energy consumption of the auxiliaries used in the propulsion cooling system is considered and two approaches are proposed to reduce it. To the author's knowledge, there are no contributions in the literature where the reduction of the energy consumption of the auxiliary loads from the propulsion cooling system is investigated. The first approach, at a design level, is modularity. The second approach, at a control level, is the optimization of the energy management.

The concept of modularity has been developed in DRIVEMODE, a project funded by the European Commission under the Horizon 2020 framework. The DRIVEMODE project stems from the idea of integrating a high-speed gearbox, a high-speed electric motor (e-motor) and a Si-C inverter to provide a highly efficient and compact integrated drivetrain module (IDM) to be used in cars of different classes, including mass produced battery and hybrid electric vehicles, low performance and high performance vehicles and different types of heavy-duty vehicles. Multiple IDM can be used in place of single larger electric machines and power electronic components. In the modules, the smaller electric machines, even though characterized by lower maximum efficiencies, will work in more efficient regions of the operating map, resulting in a lower thermal load to be rejected through the cooling system. In this paper, it is shown how modularity, among other benefits, also allows reducing the energy consumption of the cooling system.

The second approach consists of improving the energy management of the propulsion cooling system. Most of the works regarding the thermal management in electric vehicles are focused on either improving the battery cooling [15–17] or the e-motor cooling [18,19], without taking into account the cooling system energy consumption. Conventional control strategies are based on a feedback control on the radiator inlet temperature, with a thermostat valve. An interesting control approach to reduce the motor cooling system energy consumption is proposed in [20], but the considered vehicle is a hybrid electric. In this work a control strategy that reduces the energy consumption of the cooling system, namely of pump and fan, has been tuned for steady-state conditions and then tested with numerical simulation on different driving cycles. Even though the benefits of this control

strategy are smaller compared to those obtained with modularity, the implementation comes at no costs, since it does not require additional components or sensors.

This work relies on numerical simulation of experimentally validated models. Transient simulations of driving cycles have been carried out with a robust 1-D model of the vehicle cooling system built in GT-Suite [21]. On the other hand, all the thermal loads of the components of the drivetrain have been calculated with a vehicle simulator developed in Matlab/Simulink® [22].

The remainder of this paper is organized as follows: Section 2 presents the single e-motor and dual IDM configurations and modeling; Section 3 describes the cooling circuits for the two cases; finally, in Section 4 the simulations are presented, and the results are discussed; the conclusions are presented in Section 5.

## 2. System Description and Modeling

The vehicle considered in this study is an all-electric sedan-class car. The main parameters of the vehicle are listed in Table 1.

**Table 1.** Characteristics of the vehicle.

Parameter	Value
vehicle mass	1745 kg
passenger mass	235 kg
vehicle frontal cross-section area	2.618 m <sup>2</sup>
aerodynamic drag coefficient	0.29
tire rolling resistance coefficient	0.009
wheel radius	0.335 m

Two powertrain configurations are considered and further described in the next subsections: the single e-motor (with power electronics and transmission) and the dual Integrated Drivetrain Module (which incorporates e-motor, gearbox, and inverter). In both cases, the total power of the propulsion system must meet the speed and grade requirements indicated in Table 2.

**Table 2.** Performance requirements of the vehicle.

Parameter	Value
acceleration from 0 to 50 km/h	5.5 s
acceleration from 0 to 100 km/h	10 s
maximum climbing at 80 km/h	12%
maximum climbing at 130 km/h	4%
maximum speed	150 km/h

The general layout of the cooling system is composed of four integrated circuits (with a fifth separate loop for cooling charger and converters (400V-12V DC/DC and 800V-400V DC/DC)), as shown in Figure 1. The four loops are:

1. Air Conditioning (AC) refrigerant loop (shown in blue);
2. Heat Ventilation Air Conditioning (HVAC) coolant loop (shown in red);
3. Propulsion loop (shown in purple);
4. Rechargeable energy storage system (RESS) coolant loop (shown in green).

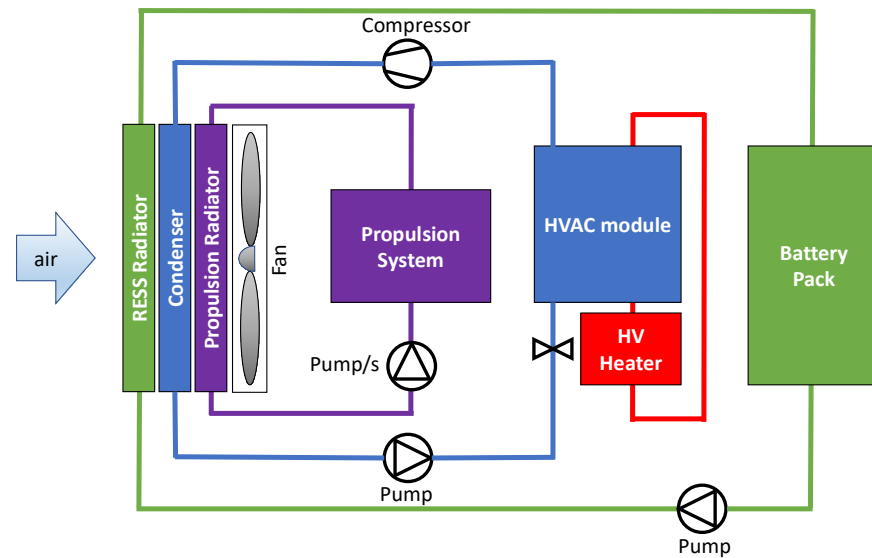


**Figure 1.** Cooling system circuits: AC refrigerant loop (blue), HVAC coolant loop (red), propulsion loop (purple), RESS loop (green).

The first loop provides air conditioning for cabin cooling through a compressed vapor cycle, whereas the second provides cabin heating. The third loop is responsible for the propulsion system cooling and the fourth loop ensures that the battery is maintained in the operating temperature range. These loops are all highly integrated, but this analysis is focused only on the propulsion coolant loop, which, however, is influenced by the HVAC refrigerant circuit through the condenser and by the RESS circuit through the RESS radiator: as shown on the left side of Figure 1, the same fan provides the air mass flow rate for the cooling of RESS, HVAC system (whose condenser is shown in blue) and propulsion module. The conditions of the air flow at the outlet of the RESS radiator and AC condenser are experimentally measured and used as an input to the simulations performed in this study.

### 2.1. Single Electric Motor

The conventional all-electric powertrain is composed of one single e-motor and one inverter. The e-motor is then connected through the transmission to the vehicle front wheels, as qualitatively shown in Figure 2.

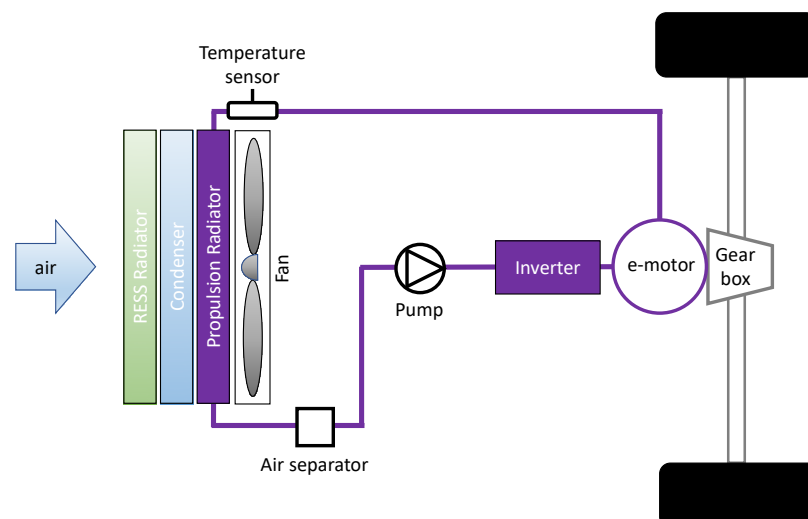


**Figure 2.** Single e-motor propulsion system and cooling system.

The electric machine has a max peak power of 150 kW and max/min continuous torque of 266 N·m, with corner speed of 1500 RPM. Figure 2 also shows the layout of the propulsion cooling system. The main components of the circuit are:

1. pipes and hoses;
2. the electric coolant pump;
3. the electric fan.

As already mentioned, the fan is used to suck in the air and increase the air mass flow rate through the radiators of propulsion, condenser and RESS cooling loops. The coolant consists of water mixed with ethylene glycol (50% water + 50% glycol).

## 2.2. Dual Integrated Drivetrain Module

Introducing the concept of modularity [23], two smaller e-motors can be used instead of the larger single motor. Each of the smaller e-motors is integrated with gearbox and Si-C inverter to form a highly efficient and compact integrated drivetrain module (IDM). Two 75 kW IDMs are used in this study to replace the single motor, as qualitatively shown in Figure 3.

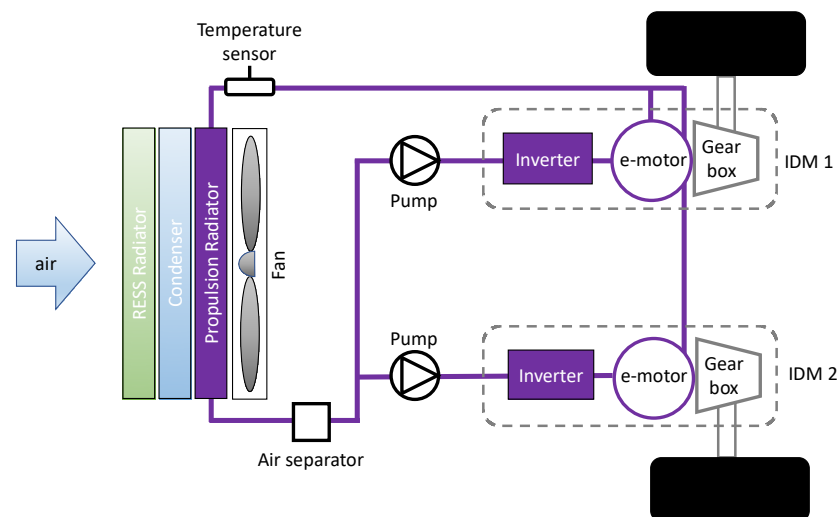


Figure 3. Dual IDM propulsion system and cooling system.

In particular, each module has a dedicated cooling circuit, with the coolant flowing through the IDM components in a series configuration. Eventually, the coolant streams coming from the two modules are sent to the same main radiator for heat rejection to the ambient. This configuration helps designing a single compact cooling circuit for the thermal management of all the propulsion components.

The benefits of modularity, i.e., using a larger number of smaller electric machines, are twofold: increased overall efficiency during the vehicle operation and reduced components heat rejection. The first benefit is explained considering that in a typical driving cycle the operating conditions will be mostly in the low-medium speeds and torques. This means that a larger EM will operate in the lower efficiency regions, while for a smaller EM most of the operating points will fall in the maximum efficiency region. Therefore, even though the larger EM could achieve greater maximum efficiency, during a driving cycle the overall efficiency of a modular propulsion system will be higher. The second benefit is strictly related to the first one, as a more efficient operation of the powertrain components will lead to less losses and heat rejection. This, in turn, will reduce the energy demand of the propulsion system cooling circuit, further improving the overall vehicle energy consumption.

### 2.3. Electric Vehicle Model

E-motor and inverter generate heat during their operation, especially at high power demands, because of ohmic losses. The cooling system is required to reject the generated thermal load to the ambient, keeping the temperatures within the operating range of the components. To evaluate the thermal load generated during the propulsion system operation, a quasi-static model of the electric vehicle has been developed in Matlab/Simulink®. The power losses in the inverter  $\dot{Q}_{INV}$ , which are equal to the heat generated, can be calculated as a function of the instantaneous inverter power  $P_{INV}$ , with the following equation:

$$\dot{Q}_{INV} = P_{INV}(1 - \eta_{INV}) \quad (1)$$

where for the inverter efficiency  $\eta_{INV}$  a constant average value equal to 97% has been used. This value results in being a bit conservative with respect to the first measurements at test bench.

On the other hand, the thermal load of the e-motor,  $\dot{Q}_{EM}$ , can be calculated as a function of the motor power,  $P_{EM}$ , and efficiency,  $\eta_{EM}$ , using the following equation:

$$\dot{Q}_{EM} = P_{EM}(1 - \eta_{EM}) \quad (2)$$

The efficiency of the single e-motor is evaluated from the map shown in Figure 4, which is obtained in [23] with the method proposed in [24].

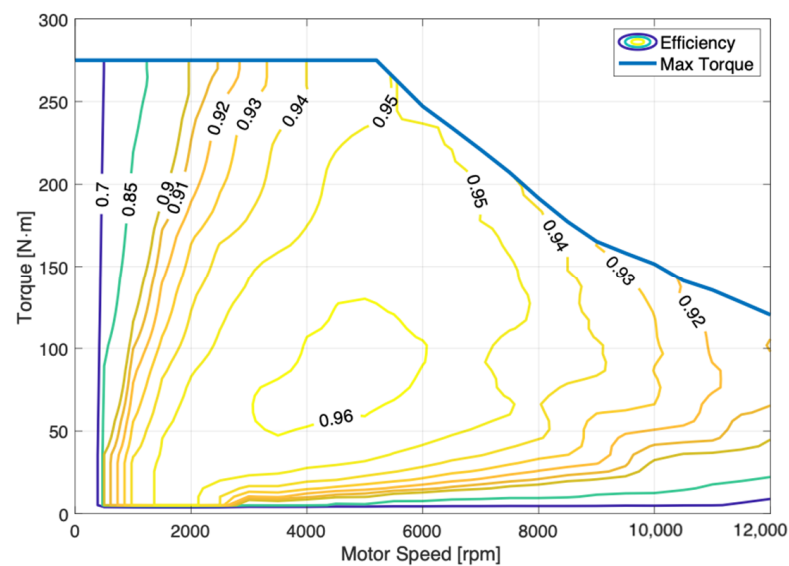


**Figure 4.** Single e-motor efficiency map.

For the e-motors of the two IDMs, the Willans line model [25] has been used to scale down the single e-motor map. The result is shown in Figure 5, with the maximum peak power of the scaled motors being one half of the maximum power of the original e-motor. Thus, the two e-motors for the dual IDM configuration have the same total power as the single e-motor configuration.

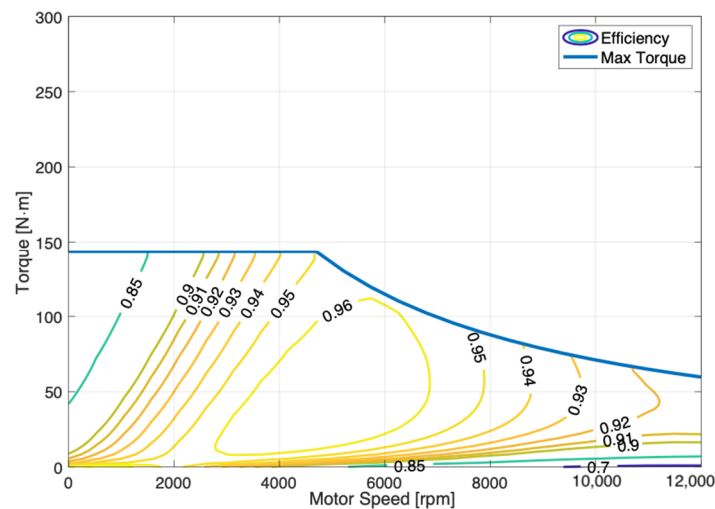


**Figure 5.** IDM e-motor efficiency map.

The maps shown in Figures 4 and 5 have been implemented in the Matlab/Simulink<sup>®</sup> model to obtain a quasi-static forward-looking simulator of the entire vehicle. The power demand on the propulsion system components is evaluated by solving the longitudinal dynamics of the vehicle and using the following expression of the road load:

$$F_{\text{load}} = \frac{1}{2} C_d \rho_{\text{air}} A_f v^2 + Mg \sin \theta + C_r Mg \cos \theta \quad (3)$$

The first term on the right-hand side of Equation (3) is the aerodynamic drag force, with  $C_d$  the drag coefficient,  $\rho_{\text{air}}$  the air density,  $A_f$  the frontal area of the vehicle and  $v$  the longitudinal speed of the vehicle. The second term is the force due to the road grade  $\theta$ , where  $g$  is the gravity constant and  $M$  is the vehicle mass. Finally, the third term is the rolling resistance force, which is a function of grade, vehicle mass and tires rolling resistance coefficient  $C_r$ . The values of these parameters have been previously reported in Table 1.

The simulator includes a driver's model based on a PID controller to track the desired speed profile (i.e., driving cycle) and a zero-th order equivalent circuit model for the battery. The main characteristics for the battery pack are listed in Table 3.

**Table 3.** Battery pack main characteristics.

Parameter	Value
operating voltage (Max/Nominal)	796/720 V DC
operating current (Max/Nominal)	280/140 A
battery capacity	46 kWh

The battery performance is obtained starting from the open circuit voltage (OCV) and internal resistance ( $R_0$ ) curves, shown in Figures 6 and 7, which have been derived from data available in [26] for a Li-Ion battery cell manufactured by A123 Systems, LCC (Livonia, MI, USA).

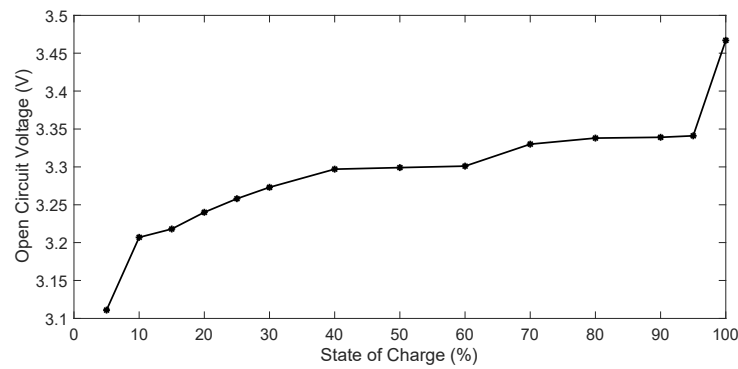


**Figure 6.** Battery cell open circuit voltage dependence on state of charge.

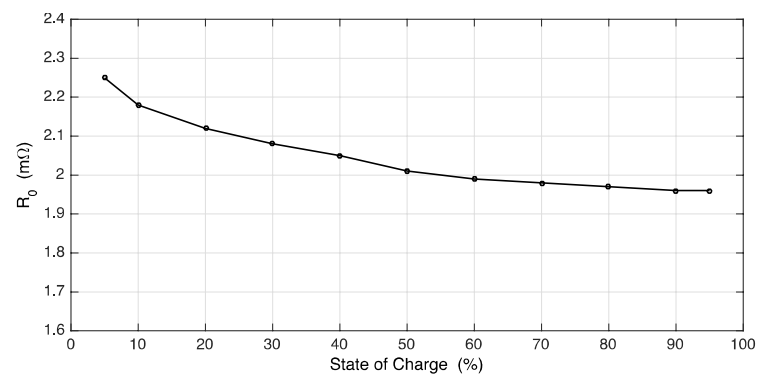


**Figure 7.** Battery cell internal resistance dependence on state of charge.

With the zero-th order equivalent circuit model the battery heat rejection,  $\dot{Q}_{batt}$ , can be calculated as:

$$\dot{Q}_{batt} = I^2 \cdot R_0(\text{SoC}) \quad (4)$$

The battery current  $I$  is a function of the battery open circuit voltage,  $V_{OC}$ , the power request,  $P_{batt}$ , and the equivalent internal resistance  $R_0(\text{SoC})$ , function of the state of charge (SoC):

$$I = \frac{V_{OC} - \sqrt{V_{OC}^2 - 4P_{batt}R_0}}{2R_0} \quad (5)$$

#### 2.4. Cooling Circuit Model

The heat rejection profiles for each component, obtained with the Matlab/Simulink® model described above, are then used as input for the propulsion cooling circuit model developed in GT-Suite and shown in Figure 8. The other input to the GT-model is the vehicle speed, which is directly related to the air flow through the cooling system radiators. Two sides or two circuits are highlighted in the model:

- Coolant side (red)—closed loop circuit with pump, accumulator, IDM components, etc.;
- Air side (blue)—circuit with Fan object, RESS and Condenser heat addition objects.

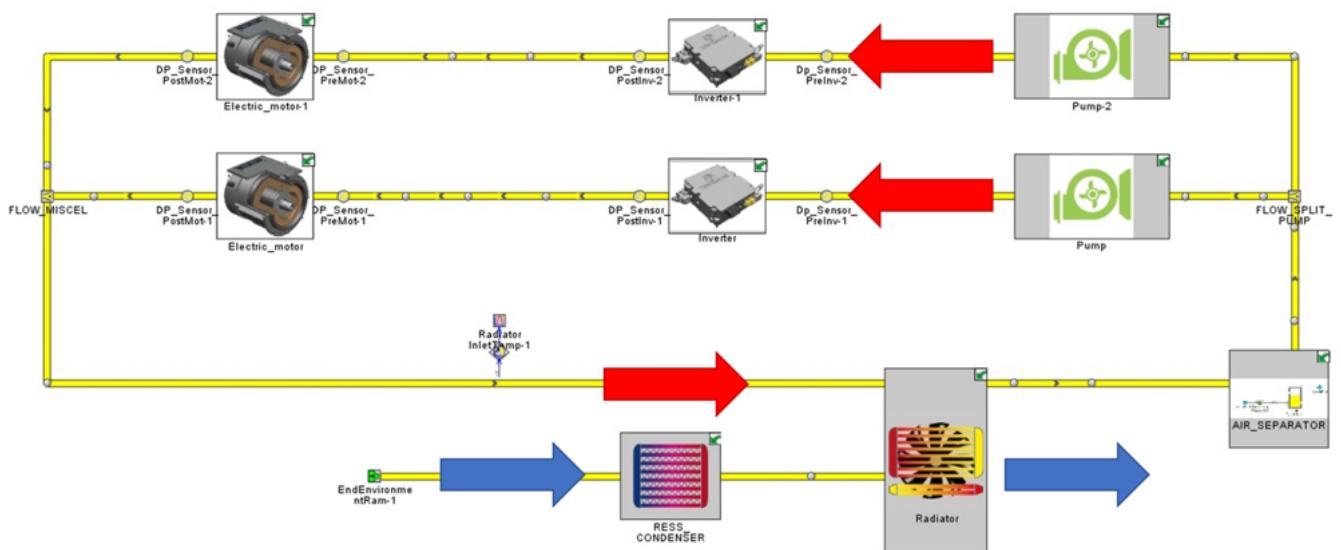


**Figure 8.** Propulsion cooling system model in GT-Suite (dual e-motor configuration).

The main components of the circuit have been modeled as follows:

- the coolant (water/glycol ethyl 50-50) properties are retrieved from the RefPROP [27] library;
- pipes and hoses, whose dimensions are the results of a sensitivity analysis aiming to minimize the circuit pressure drops and ensuring the required mass flow rate for cooling, have inner diameter of 19 mm, locally 18 mm in some connectors;
- the coolant pump, which is an electric pump, is modeled with the operating map shown in Figure 9;
- the electric fan, modeled with the operating map shown in Figure 10.

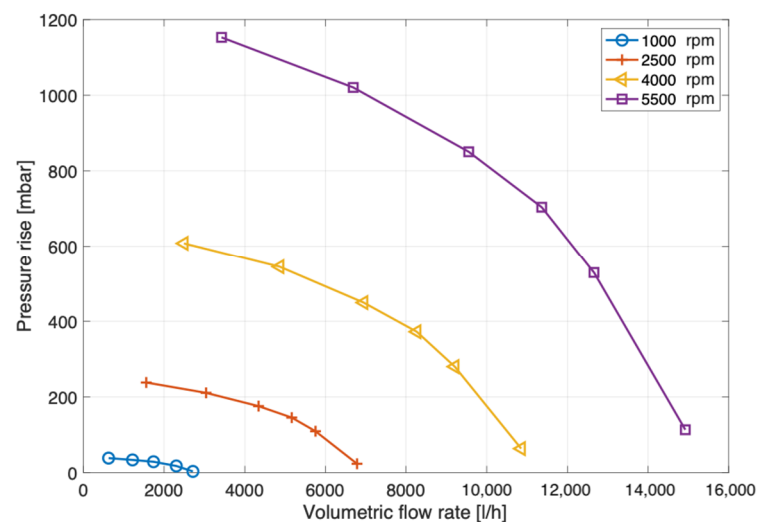


**Figure 9.** Cooling system pump map.

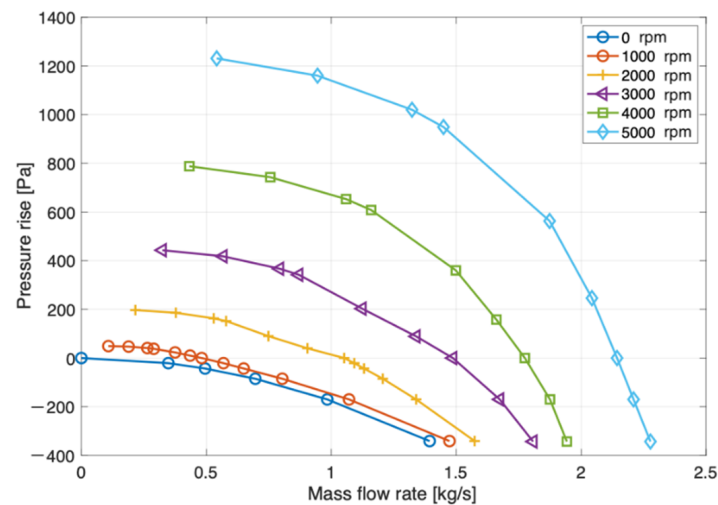


Figure 10. Cooling system fan map.

Additionally, the thermal load of the propulsion radiator is an output of the analysis rather than an input. All the data needed to model the heat transfer behavior of the radiator have been provided by the car manufacturer. The performance that the propulsion cooling system must meet are summarized in Table 4. In particular, the temperature must not exceed 65 °C. In the case of the dual IDM the constraint on the minimum volumetric flow rate imposes the usage of two pumps. This has been found to be consistent with the modularity requirement of the DRIVEMODE project, since each module comes with its own pump.

Table 4. Preliminary requirements for the cooling circuit.

<b>e-motor</b>	
temperature (inlet)	<65 °C
pressure drop	<500 mbar @ 10 L/min
vol. flow rate	>10 L/min @ maximum power
<b>inverter</b>	
temperature (inlet)	<65 °C
pressure drop	<300 mbar @ 10 L/min
vol. flow rate	>10 L/min @ maximum power

### 3. Cooling Circuit Control Strategy

The second approach to reduce the energy consumption from the auxiliary loads related to the propulsion cooling system consists of optimizing the control strategy of fan and pump. The fan is responsible for increasing the air flow through the radiator, thus improving the heat rejection when the driving loads are high. The pump is used to ensure the desired flow of coolant through the propulsion system components and keep their temperature in the admissible range. In the following subsections, the conventional control strategy and the proposed optimized strategy are presented. Both strategies apply to either the single e-motor or the dual IDM configurations.

#### 3.1. Conventional Control

The conventional control strategy acts on two control variables, which are the pump speed, and the input signal of the fan (on/off). The pump speed is initially set at 10 L/min and then it is linearly increased as the coolant temperature at the radiator inlet increases above 40 °C. The fan is off as long as this temperature is below 65 °C. For higher values, the fan is switched on at its maximum capacity (i.e., input signal equal to 90%) and is maintained on until the temperature drops down below 55 °C, performing a hysteresis

cycle. When the radiator inlet temperature reaches 65 °C and the fan is turned on, the pump flow rate is kept constant at its maximum value. The linear dependency of the pump speed (proportional to the pump flow rate) on the coolant temperature at the radiator inlet is shown in Figure 11. The minimum pump speed corresponds to 10 L/min, as per the constraint reported in Table 4, while the maximum volumetric flow rate is obtained for the maximum pump speed.

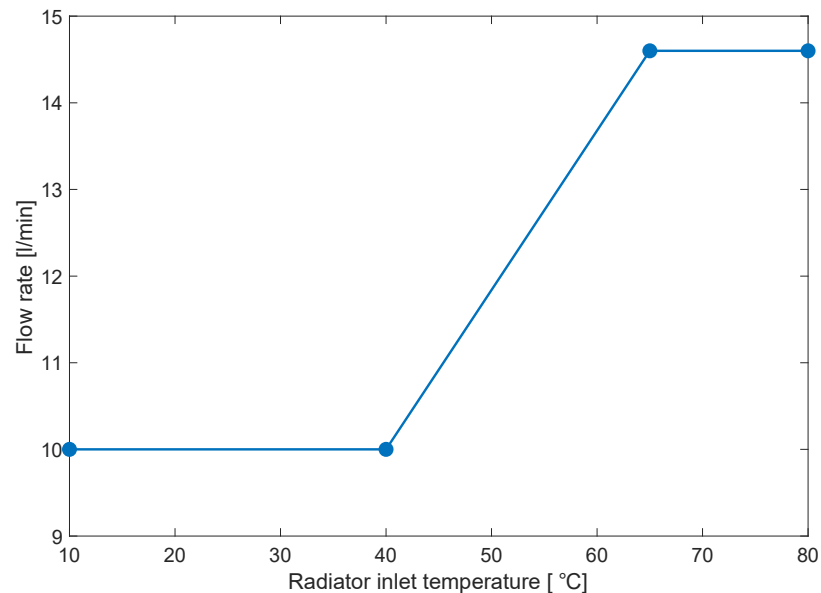


**Figure 11.** Pump conventional control strategy: linear dependence of mass flow rate on coolant temperature at radiator inlet.

### 3.2. Optimized Control

The optimized control strategy aims at reducing the energy consumption of pump and fan, ensuring the temperature constraints on the e-motor and inverter are met. In contrast with the conventional strategy, in this case the speed of the pumps is controlled based on the actual vehicle speed, actual heat rejection of the components and fan state. These signals are already available in the vehicle, as they are used for other tasks of the electronic control unit, so no additional sensors are required to implement the new control strategy.

The control strategy is built on the observation that for a given vehicle speed and thermal load on the cooling circuit, the pump speed corresponding to the minimum energy consumption is the lowest possible speed that avoids the fan to be switched on. Therefore, an optimization process has been carried out to evaluate the minimum pump speed required to reject different thermal loads at different vehicle speeds, without turning on the fan. A design of the experiment was performed with the Matlab/Simulink® simulator, varying vehicle speed and road grade to obtain the heat rejection of the components for different road load conditions. Those results were then used for steady-state simulations of the 1-D GT-Suite cooling circuit together with built in optimization algorithms from GT-Suite to create the control map shown in Figure 12. For the same vehicle speed, higher loads correspond to higher heat rejections and require higher mass flow rates (thus, pump speeds).

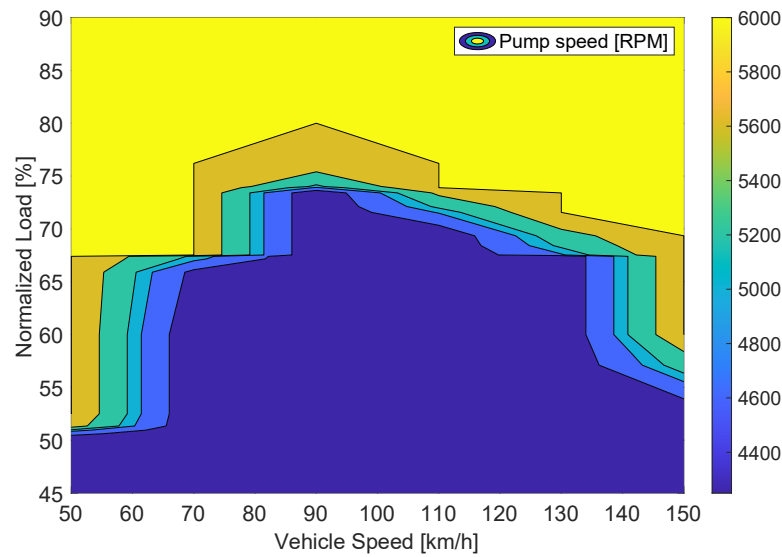


**Figure 12.** Optimized control strategy: optimized pump speed as a function of vehicle speed and propulsion normalized load.

The map shows a step-shape because the pump speed has a low impact on the coolant temperature. Indeed, the most important variables for the heat transfer in the radiator are the air mass flow rate and the air temperature, which are influenced by vehicle speed and fan state. In other words, for the same level of required heat rejection, while the speed of the pumps can only produce a small change of the radiator inlet temperature, the fan state and vehicle speed can have a much greater impact. As a result, there is no advantage in maintaining high pump speeds during the fan operation, because the main contribution to lowering the temperature is from the fan, and the increasing fan operational time is negligible. Following this consideration, the optimal pump speed from the map is overwritten when the fan is turned on, setting the speed to its minimum value.

In the first step of the control strategy, the calculation of the pump speed is only based on the actual vehicle speed (i.e., air flow rate through the radiator) and heat rejection from the components, using the control map shown in Figure 12, which is embedded into a 2D lookup table. The actual optimal speed output signal from the 2D lookup table is time averaged to smooth speed variations. This is necessary to dampen the dynamics of the inputs to the lookup table, which is built from steady-state simulations.

In a second step, the actual coolant temperature at the radiator inlet is checked. If the temperature of the coolant exceeds 60 °C, then the fan is turned on and the minimum pump speed is imposed, overwriting the optimal speed output of the 2D lookup table. The fan performs the same hysteresis cycle between 60 °C and 55 °C as already described in the previous section.

To summarize, the control strategy is designed to optimize the speed of the pump(s) when the fan is off, and to set it to the minimum allowed value when the fan is on:

$$n_{\text{pump}}(x_{\text{fan}}, \dot{Q}_{\text{loss}}, v_{\text{vehicle}}) = \begin{cases} \bar{n}_{\text{pump}}(\dot{Q}_{\text{loss}}, v_{\text{vehicle}}), & x_{\text{fan}} = 0 \\ n_{\text{pump}} = 4250 \text{ rpm}, & x_{\text{fan}} = 1 \end{cases} \quad (6)$$

where  $x_{\text{fan}}$  is the actual state of the fan, equal to 1 if the fan is on and equal to 0 if the fan is off;  $\dot{Q}_{\text{loss}}$  represents the total heat rejection of the components that is a function of time;  $v_{\text{vehicle}}$  is the actual vehicle speed;  $n_{\text{pump}}$  is the speed of the pump and  $\bar{n}_{\text{pump}}$  is the time averaged value of  $n_{\text{pump}}$  coming from the optimized control map. After a sensitivity analysis the averaging time of  $\bar{n}_{\text{pump}}$  has been set equal to 25 s for all the simulations.

#### 4. Simulations and Results

To investigate the operation and performance of the cooling system, three different driving cycles (i.e., vehicle speed time profiles) have been selected: Aachen drive cycle, shown in Figure 13a; Federal Highway Driving Schedule (FHDS) drive cycle (repeated 10 times), shown in Figure 13b; World harmonized Light-duty vehicles Test Procedure (WLTC) drive cycle (repeated 3 times), shown in Figure 13c.

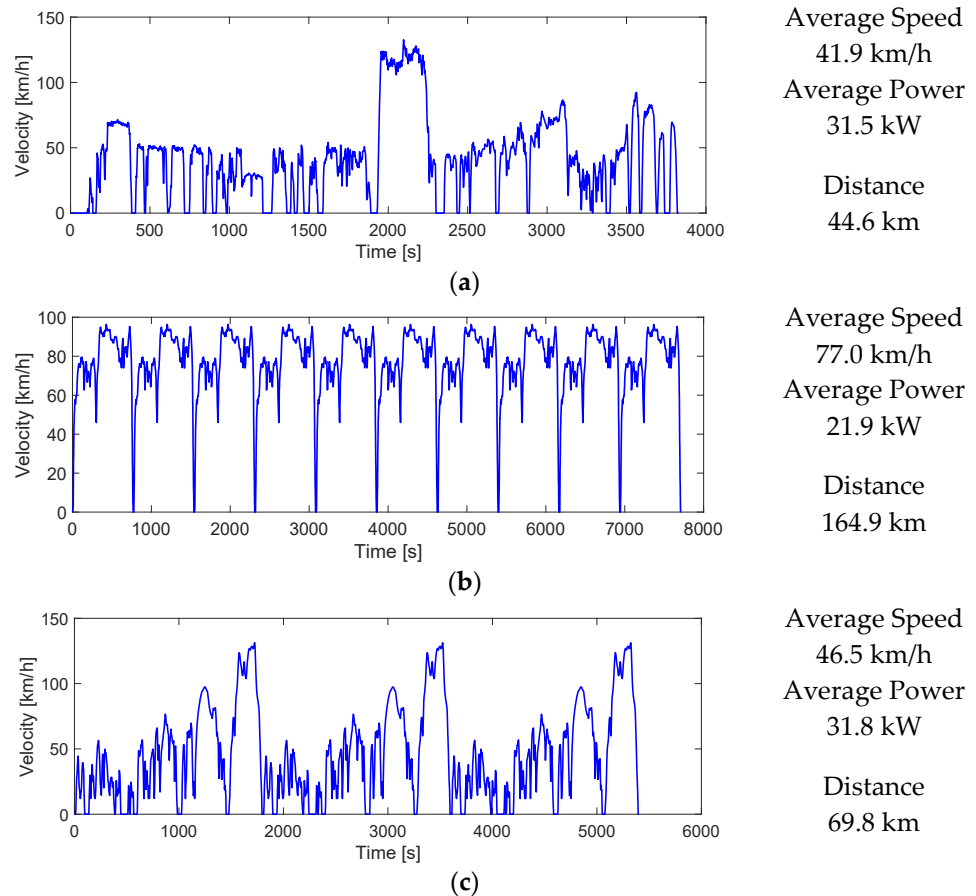


**Figure 13.** Test driving cycles: (a) Aachen; (b) FHDS  $\times$  10; (c) WLTC  $\times$  3.

The cycle repetitions are needed to obtain the same cooling circuit operating time and realistic trip length. Also, to add variability to the road power demand, each cycle repetition is characterized by a different road grade profile.

In the Matlab/Simulink<sup>®</sup> forward-looking model both the single motor and dual IDM configurations were simulated for the three driving cycles. The main outputs of these simulations are the heat rejection profile of the components and the effective vehicle speed. The operating average efficiency of the e-motors for the different driving cycles and the different powertrain architectures is reported in Table 5. It is clear that the modularity can improve the operating efficiency of the e-motors, thus reducing the heat generation that the cooling circuit will have to reject to the ambient.

**Table 5.** E-motor average efficiency.

Driving Cycle	Single e-motor EM Efficiency (%)	Dual IDM EM Efficiency (%)
Aachen	82.8	92.6
FHDS $\times$ 10	83.5	88.4
WLTC $\times$ 3	88.4	93.5

The heat rejection profile and the vehicle speed are then used as inputs to the GT-Suite model, which solves the transient 1-D thermo-fluid dynamic problem and evaluates the performance of the cooling circuit. Both the conventional and the optimized control strategy for the pump(s) control are simulated.

The effectiveness of the control strategies has been tested under the following additional assumptions: constant gear box efficiency of 0.97; mass of the vehicle equal to the gross weight; no AC condenser heat rate; ambient temperature of 40 °C; coolant initial temperature of 40 °C. These extreme operating conditions have been chosen to stress the cooling system and trigger fan starting events. As an example, Figure 14 shows the heat rejections of the motor, inverter, and battery with respect to time for the WLTC  $\times$  3 cycle.

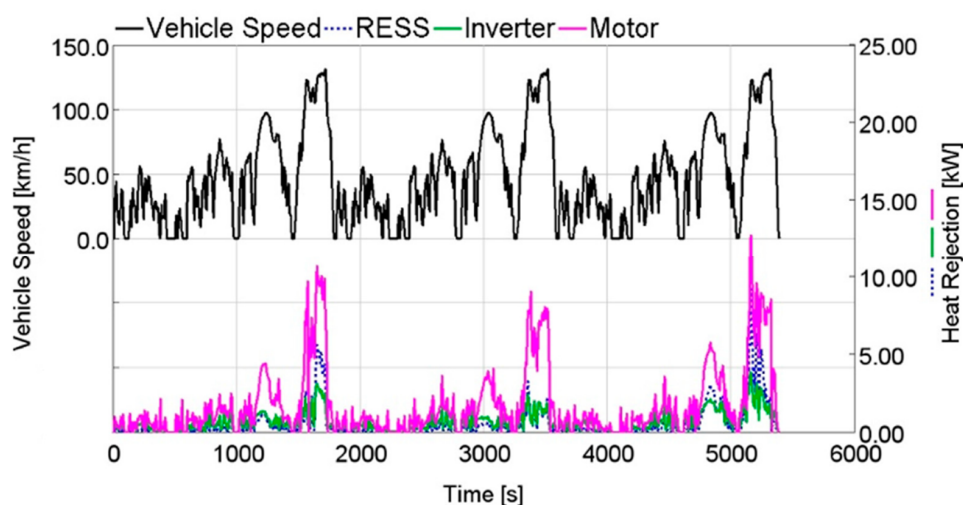


**Figure 14.** Outputs of the all-electric vehicle model: actual vehicle speed profile (top); motor, inverter and RESS heat rejections vs. time (bottom).

As one may note, there is a correlation between the velocity profile and the heat rejection, which is obviously affected by the road load. These plots are mostly provided to prove the soundness of the energy-based vehicle simulator. Those heat rejections have been calculated with the set of equations from (1) to (4).

#### Results Discussion and Comparison

To understand the impact of modularity and optimized control strategy on the energy consumption reduction, four cases have been analyzed for every driving cycle:

1. Single e-motor, standard propulsion cooling management;
2. Single e-motor, optimized propulsion cooling management;
3. Dual IDM, standard propulsion cooling management;
4. Dual IDM, optimized propulsion cooling management.

The different driving cycles highlight different aspects of the powertrain configurations and control strategies.

For the WLTC  $\times$  3 drive cycle, the speeds of pump and fan (which can be considered to be a measure of the energy consumption) are shown in Figures 15 and 16 for the single e-motor and the dual IDM configurations, respectively. The WLTC  $\times$  3 is the most power demanding driving cycle and in all the cases the fan must be activated to lower the coolant temperature. Moreover, comparing Figures 15 and 16, the single e-motor configuration requires one more fan start due to the higher heat rejection of the components in this powertrain.

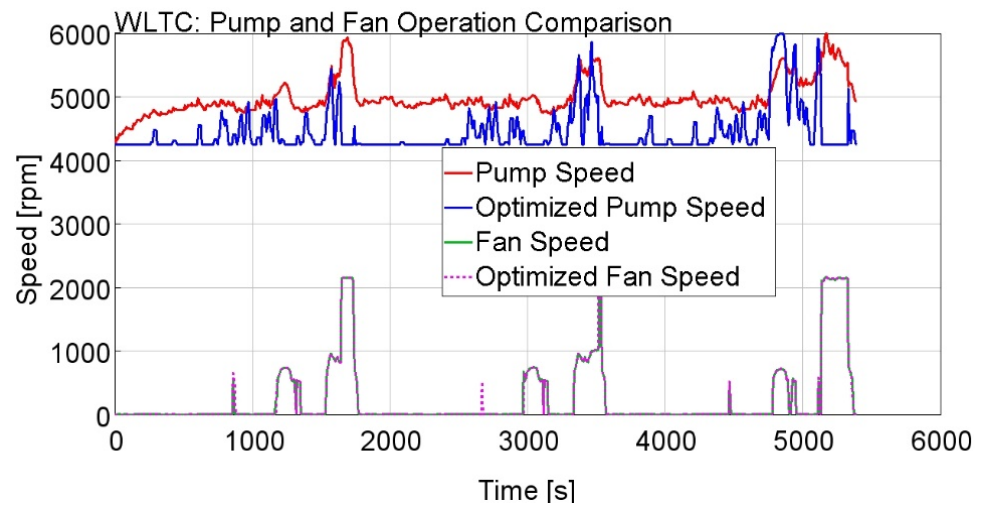


**Figure 15.** Control strategy comparison for single e-motor on WLTC driving cycle: coolant pump speed (top); radiator fan speed (bottom).

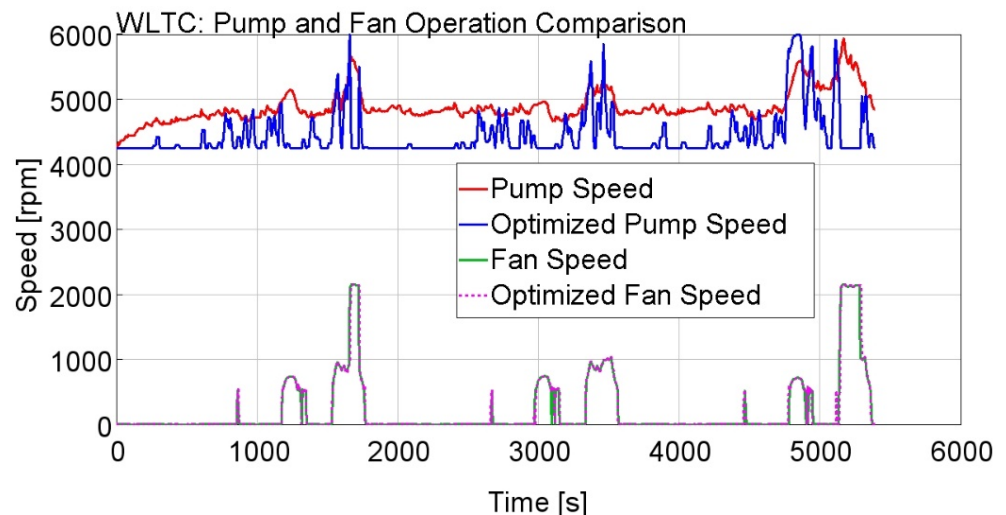


**Figure 16.** Control strategy comparison for dual IDM on WLTC driving cycle: coolant pump speed (top); radiator fan speed (bottom).

The bar plot in Figure 17 allows a comparison among the energy consumptions of every component, for both configurations and control strategies. The optimized control strategy for the dual IDM leads to higher fan energy consumption compared to the conventional strategy because the minimum pump speed is imposed during the fan operation time. However, the overall energy consumption is still better for the optimized control strategy because the energy savings of the pumps are much greater than the increased fan consumption. This confirms that the contribution of the fan on lowering the coolant temperature is prominent with respect to the pump. Furthermore, setting the pumps at the minimum speed leads to only a few seconds of fan additional operating time. For a specific powertrain (e.g., either Figure 15 or Figure 16), it is difficult to observe the differences in the fan operation times, since the pump(s) only have a limited impact on the coolant temperature. However, the difference between conventional and optimized control strategy is evident in terms of pump speed. As expected, the optimized control strategy is able to minimize the pump(s) speed, thus their energy consumption during most of the trip length.

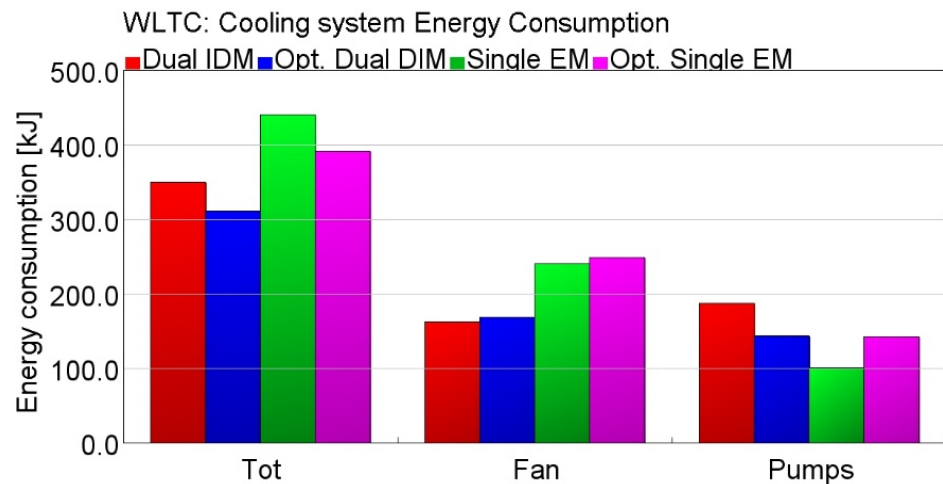


**Figure 17.** Impact of modularity and optimized control strategy on the energy consumption reduction for the WLTC driving cycle.

Regarding the temperature profiles at the radiator inlet, Figure 18 shows the differences for the four cases.

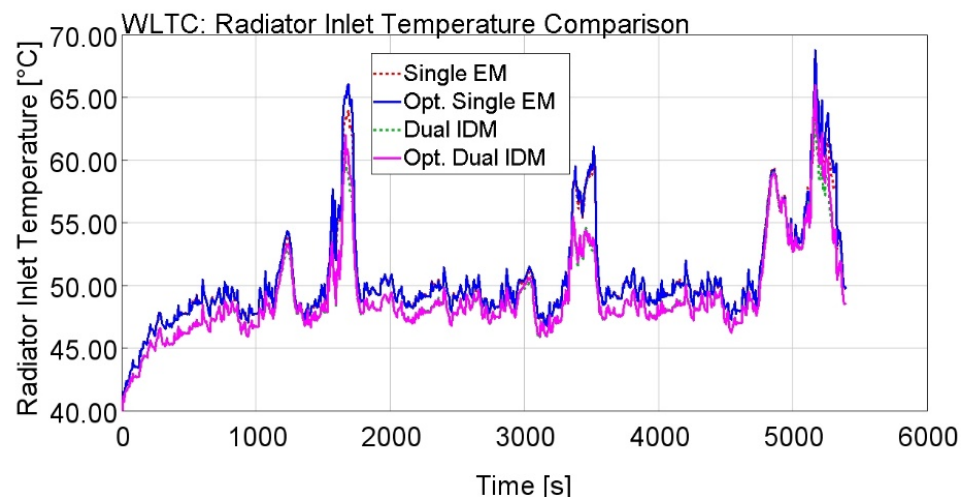


**Figure 18.** Impact of modularity and optimized control strategy on the coolant temperature at the radiator inlet for the WLTC driving cycle.

The difference in the shape of the peaks (see left plots in Figure 18) is caused by the difference in the actual battery state of charge and grade conditions for the three repetitions, leading to different maximum heat rejections. Because of the high energy demand and road grade, the single e-motor configuration is not able to meet the radiator inlet temperature constraint and both conventional and optimized control strategy lead to temperatures higher than 65 °C during the heat rejection peaks. On the other hand, the dual IDM configuration always meets the constraint with the conventional controller, while the optimized controller slightly exceeds 65 °C for 20 s. Comparing the four cases, the temperature is lower in the dual IDM configuration during the whole trip and there is no temperature difference between optimized and conventional control strategy when the fan is turned off.

The results for the FHDS drive cycle that is the less power demanding cycle, are shown in Figures 19–22.

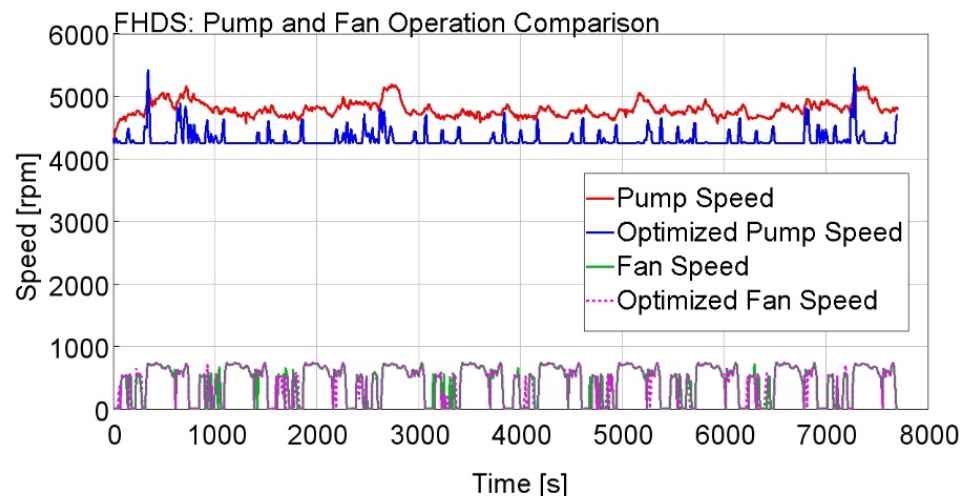


Figure 19. Control strategy comparison for single e-motor on FHDS driving cycle: coolant pump speed (top); radiator fan speed (bottom).

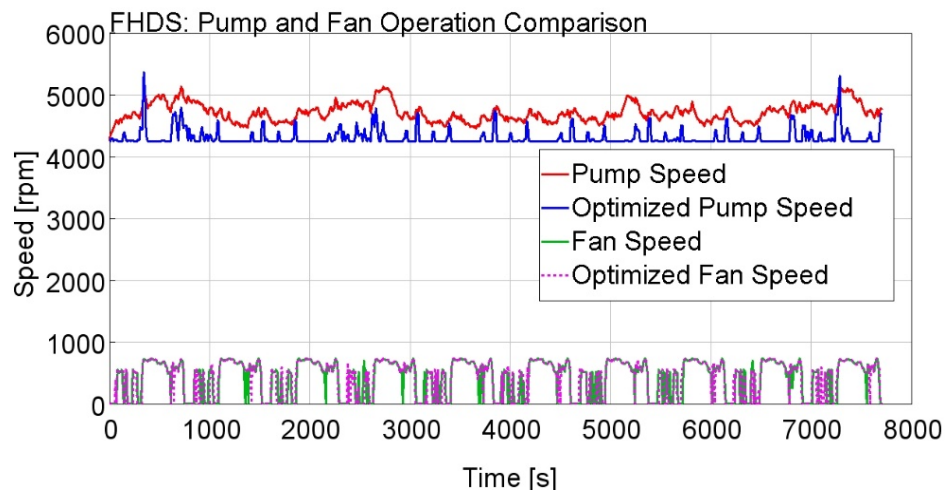


Figure 20. Control strategy comparison for dual IDM on FHDS driving cycle: coolant pump speed (top); radiator fan speed (bottom).

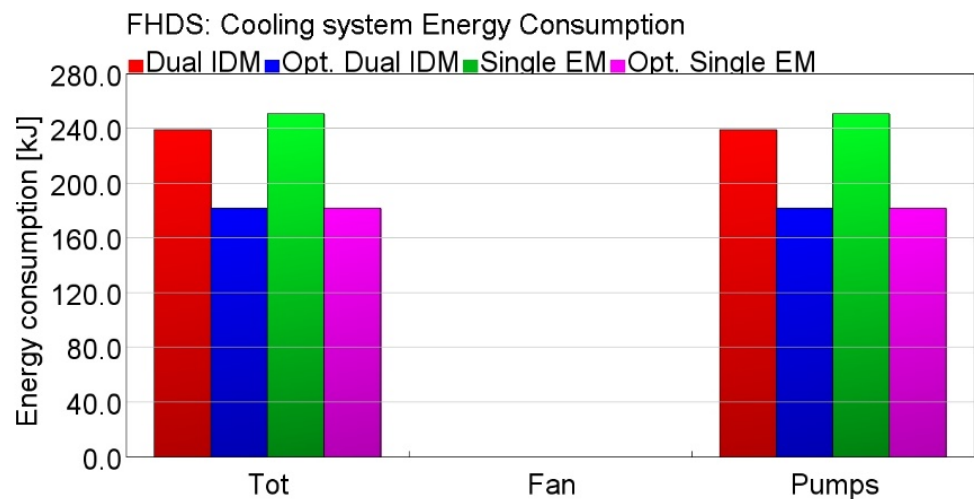
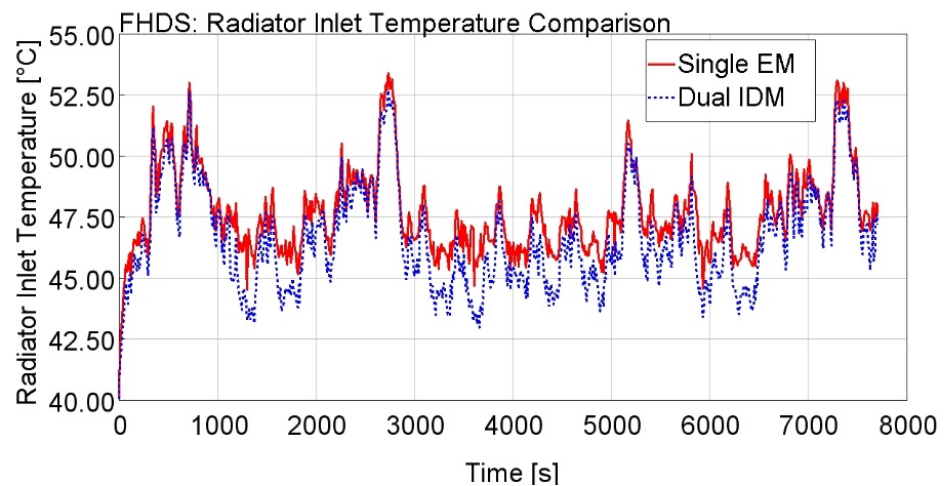


Figure 21. Impact of modularity and optimized control strategy on the energy consumption reduction for the FHDS driving cycle.



**Figure 22.** Impact of modularity and optimized control strategy on the coolant temperature at the radiator inlet for the FHDS driving cycle.

Even though Figures 19 and 20 show a non-zero fan speed, in both cases the fan is never switched on and the reported speeds result from the vehicle speed dragging the fan blades and producing the so-called “windmill” effect. This results in a clear energy saving for the optimized control strategy, as shown in the bar plot in Figure 21. In this driving cycle, the optimized control map leads to lower average speeds, thus the pump(s) give a significant contribution to the energy consumption reduction, while the conventional control strategy sets a high speed on average because the coolant temperature is in the range 50–55 °C most of the time, as shown in Figure 22, resulting in higher energy consumptions. Figure 22 also shows that for each powertrain configuration, the optimized control strategy leads to nearly the same temperature as the conventional strategy, such that the two temperature profiles overlap, and only one profile is shown in Figure 22. It can be concluded that in medium-low road power demand conditions the optimized control strategy can reduce the propulsion cooling system energy consumption.

Finally, for the Aachen driving cycle, the simulation results are shown in Figures 23–26. In this case, a large difference is found for the two powertrain configurations. In general, these simulations show how modularity can reduce the total heat rejection thanks to the higher operating efficiency of the 2 IDMs, therefore the cooling system is less stressed and energy consumption is lower. Comparing Figures 23 and 24, the dual IDM configuration never turns on the fan (also in this case the speed of the fan is due to windmill effect), while the single e-motor requires multiple fan starts. Looking at Figure 23, for the single e-motor the operation time of the fan is longer with the optimized control strategy, due to the lower pump speed imposed during the fan operation time. However, this little drawback is canceled out by the lower optimized pump speed (thus energy consumption) during the whole trip length.

Finally, the consumptions for the Aachen drive cycle are summarized in the bar plot in Figure 25. Regarding the temperatures, Figure 26 shows in detail the temperature difference between optimized and conventional control strategy, with slightly higher temperatures for the optimized strategy, which in turn result in lower energy consumptions, still meeting the cooling requirements.

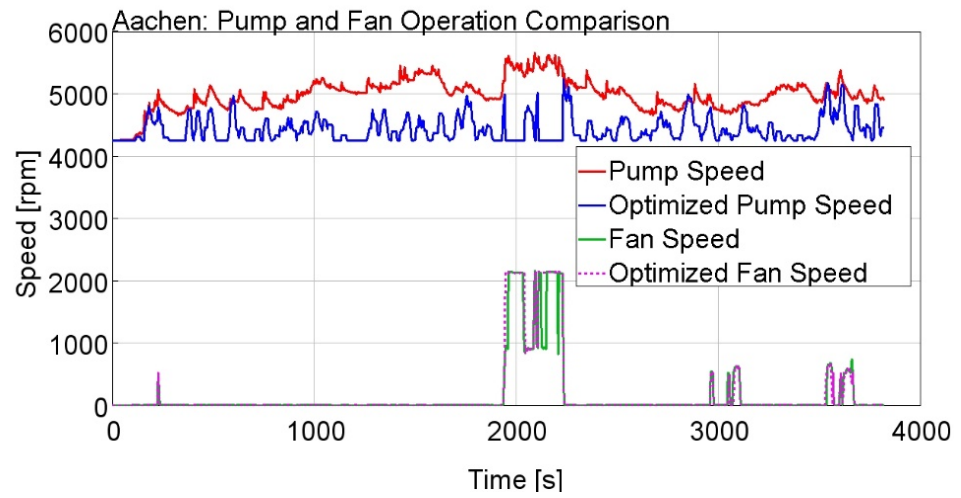


Figure 23. Control strategy comparison for single e-motor on Aachen driving cycle: coolant pump speed (top); radiator fan speed (bottom).

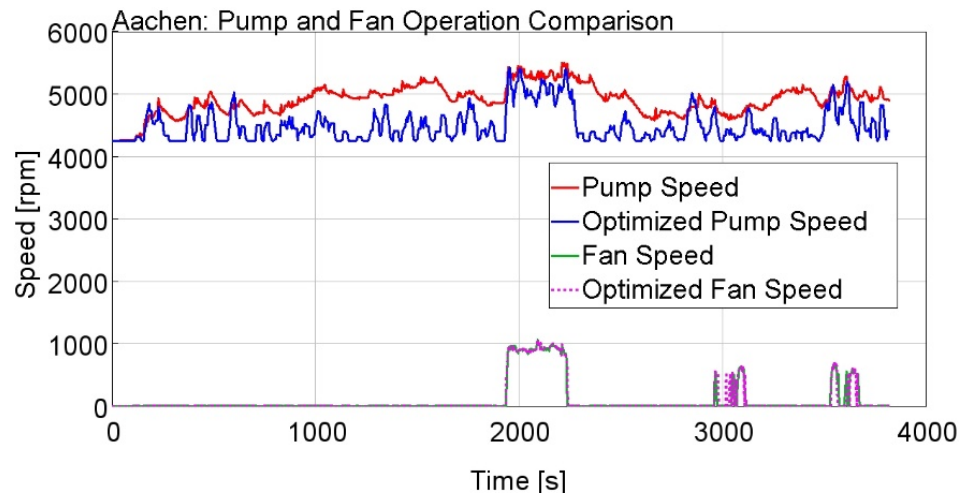


Figure 24. Control strategy comparison for dual IDM on Aachen driving cycle: coolant pump speed (top); radiator fan speed (bottom).

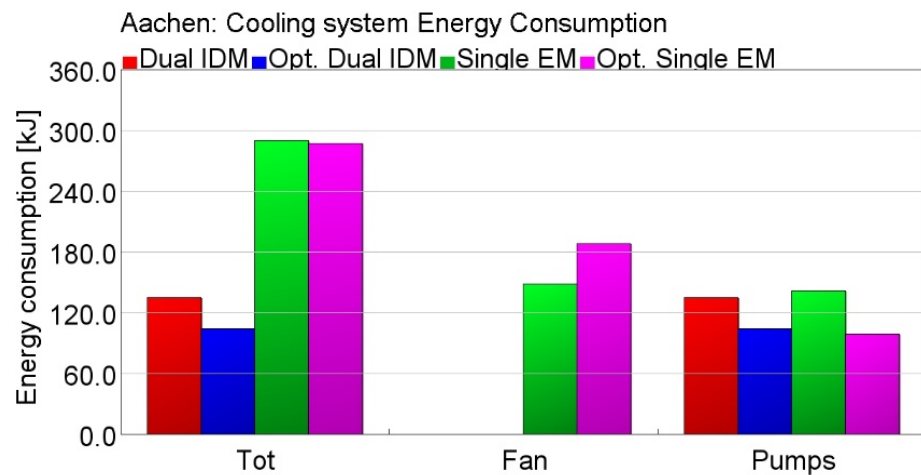
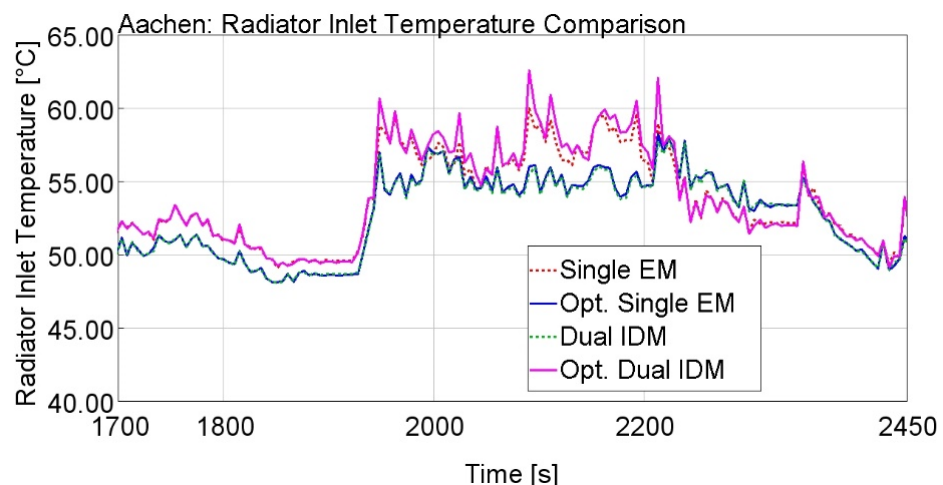


Figure 25. Impact of modularity and optimized control strategy on the energy consumption reduction for the Aachen driving cycle.



**Figure 26.** Impact of modularity and optimized control strategy on the coolant temperature at the radiator inlet for the Aachen driving cycle.

## 5. Conclusions

Methods to reduce the propulsion system cooling circuit energy consumption in an all-electric vehicle have been investigated in this paper. To achieve the goal of reducing the energy consumption of the auxiliaries that actuate the propulsion cooling system, both improvement of the powertrain efficiency and optimization of the cooling system control strategy have been analyzed. In particular, the improvement of the powertrain efficiency is obtained with a dual integrated drivetrain module configuration, which allows for lower heat rejection from the drivetrain components. On the other hand, an optimized control strategy for the cooling system has been designed in order to minimize the power demand of the cooling system. The cooling system simulations have been carried out with a 1-D model built upon experimental data in GT-Suite, while a vehicle simulator developed in Matlab/Simulink<sup>®</sup> has been used to evaluate the thermal loads of the components under different driving cycles. From the analysis of the results presented in the previous section, the following conclusions can be drawn:

1. The dual IDM configuration leads to an overall efficiency improvement due to the increased average efficiency of the e-motors, which intrinsically results in lower heat rejection and lower energy demand from the propulsion cooling system. However, in terms of energy consumption reduction of the propulsion system cooling circuit, the benefit of the dual IDM configuration steps out only in severe load conditions that stress the cooling circuit and trigger the fan. Indeed, for the FHDS driving cycle, the single e-motor and dual IDM have similar performance in terms of cooling circuit energy consumption. In this case, compared to the single e-motor configuration, modularity achieves only a 5% reduction of energy consumption. However, in the WLTCx3 and Aachen driving cycles, modularity results in a 21% and 54% reduction of energy consumption of the propulsion cooling system compared to the single e-motor configuration, respectively.
2. The optimized control strategy implemented in the propulsion cooling management always leads to lower energy consumption. The effectiveness of the control strategy comes from the reduction of the energy consumption of the cooling circuit pumps. Because of this, the optimized propulsion cooling management steps out in medium load conditions, when the control of the speed of the pumps is needed to lower the coolant temperature, but no action from the fan is requested. Indeed, when the fan is turned on, it will increase the overall consumption of the cooling circuit, decreasing the relative weight of the pumps on the consumption and consequently decreasing the impact of the optimized control strategy. In the Aachen driving cycle, compared to the single e-motor, the optimal control strategy achieves a 1% energy consumption

reduction, whereas 11% and 27% reductions are achieved for the WLTCx3 and FHDS driving cycles, respectively.

As a consequence of conclusions 1 and 2, in order to decrease the auxiliary loads of the propulsion cooling system in all-electric powertrains, increasing the powertrain efficiency leads to good results only if the cooling circuit is stressed enough, or in other words, if the fan is activated during the vehicle operation. On the other hand, the optimization of the control strategy is relevant if normally the cooling circuit is capable of lowering the coolant temperature without the intervention of the fan.

**Author Contributions:** Conceptualization: S.L., M.V., D.C. and L.T.; Formal analysis, S.L., M.V., D.C. and L.T.; Investigation, S.L. and L.T.; Methodology, M.V. and L.T.; Project administration, D.C. and L.T.; Software, S.L.; Supervision, D.C. and L.T.; Validation, S.L.; Visualization, M.V.; Writing—original draft, M.V.; Writing—review & editing, M.V., D.C. and L.T. All authors have read and agreed to the published version of the manuscript.

**Funding:** This project has received funding from the European Union’s Horizon 2020 research and innovation program under grant agreement No 769989. The opinions expressed in this document reflect only the author’s view and reflects in no way the European Commission’s opinions. The European Commission is not responsible for any use that may be made of the information it contains.

**Institutional Review Board Statement:** Not applicable.

**Informed Consent Statement:** Not applicable.

**Data Availability Statement:** The data presented in this study are possibly available on request from the corresponding authors. The data are not publicly available due to confidentiality reasons.

**Conflicts of Interest:** The authors declare no conflict of interest.

## References

- Varga, B.; Sagoian, A.; Mariasiu, F. Prediction of Electric Vehicle Range: A Comprehensive Review of Current Issues and Challenges. *Energies* **2019**, *12*, 946. [[CrossRef](#)]
- Michaelides, E.E. Thermodynamics and energy usage of electric vehicles. *Energy Convers. Manag.* **2020**, *203*, 112246. [[CrossRef](#)]
- Iora, P.; Tribioli, L. Effect of Ambient Temperature on Electric Vehicles’ Energy Consumption and Range: Model Definition and Sensitivity Analysis Based on Nissan Leaf Data. *World Electr. Veh. J.* **2019**, *10*, 2. [[CrossRef](#)]
- Samadani, E.; Fraser, R.; Fowler, M. Evaluation of air conditioning impact on the electric vehicle range and li-ion battery life. *SAE Tech. Pap.* **2014**, *1*. [[CrossRef](#)]
- Rugh, J.; Farrington, R. *Vehicle Ancillary Load Reduction Project Close-Out Report: An Overview of the Task and a Compilation of the Research Results*; National Renewable Energy Laboratory: Golden, CO, USA, 2008.
- Gao, G. Investigation of climate control power consumption in DTE estimation for electric vehicles. *SAE Tech. Pap.* **2014**, *1*. [[CrossRef](#)]
- Kambly, K.R.; Bradley, T.H. Estimating the HVAC energy consumption of plug-in electric vehicles. *J. Power Sources* **2014**, *259*, 117–124. [[CrossRef](#)]
- Lahlou, A.; Ossart, F.; Boudard, E.; Roy, F.; Bakhouya, M. Optimal Management of Thermal Comfort and Driving Range in Electric Vehicles. *Energies* **2020**, *13*, 4471. [[CrossRef](#)]
- Desreveaux, A.; Bouscayrol, A.; Castex, E.; Trigui, R.; Hittinger, E.; Sirbu, G.-M. Annual Variation in Energy Consumption of an Electric Vehicle Used for Commuting. *Energies* **2020**, *13*, 4639. [[CrossRef](#)]
- Basciotti, D.; Dvorak, D.; Gellai, I. A Novel Methodology for Evaluating the Impact of Energy Efficiency Measures on the Cabin Thermal Comfort of Electric Vehicles. *Energies* **2020**, *13*, 3872. [[CrossRef](#)]
- Wang, Y.; Gao, Q.; Zhang, T.; Wang, G.; Jiang, Z.; Li, Y. Advances in integrated vehicle thermal management and numerical simulation. *Energies* **2017**, *10*, 1636. [[CrossRef](#)]
- Shojaei, S.; Robinson, S.; McGordon, A.; Marco, J. Passengers vs. Battery: Calculation of Cooling Requirements in a PHEV. *SAE Tech. Pap.* **2016**, 2016. [[CrossRef](#)]
- Titov, G.; Aaron Lustbader, J. Modeling Control Strategies and Range Impacts for Electric Vehicle Integrated Thermal Management Systems with MATLAB/Simulink. In Proceedings of the WCX17: SAE World Congress Experience, Detroit, MI, USA, 4–6 April 2017.
- Chowdhury, S.; Leitzel, L.; Zima, M.; Santacesaria, M. Total Thermal Management of Battery Electric Vehicles (BEVs). *SAE Tech. Pap.* **2018**. [[CrossRef](#)]
- Wu, W.; Wang, S.; Wu, W.; Chen, K.; Hong, S.; Lai, Y. A critical review of battery thermal performance and liquid based battery thermal management. *Energy Convers. Manag.* **2019**, *182*, 262–281. [[CrossRef](#)]
- Arasu, M.; Ahmed, Q.; Rizzoni, G. Optimizing battery cooling system for a range extended electric truck. *SAE Tech. Pap.* **2019**, 2019, 1–9. [[CrossRef](#)]

17. Kong, D.; Peng, R.; Ping, P.; Du, J.; Chen, G.; Wen, J. A novel battery thermal management system coupling with PCM and optimized controllable liquid cooling for different ambient temperatures. *Energy Convers. Manag.* **2020**, *204*, 112280. [[CrossRef](#)]
18. Davin, T.; Pellé, J.; Harmand, S.; Yu, R. Experimental study of oil cooling systems for electric motors. *Appl. Therm. Eng.* **2015**, *75*, 1–13. [[CrossRef](#)]
19. Fang, G.; Yuan, W.; Yan, Z.; Sun, Y.; Tang, Y. Thermal management integrated with three-dimensional heat pipes for air-cooled permanent magnet synchronous motor. *Appl. Therm. Eng.* **2019**, *152*, 594–604. [[CrossRef](#)]
20. Huang, J.; Naini, S.S.; Miller, R.; Rizzo, D.; Sebeck, K.; Shurin, S.; Wagner, J. A Hybrid Electric Vehicle Motor Cooling System—Design, Model, and Control. *IEEE Trans. Veh. Technol.* **2019**, *68*, 4467–4478. [[CrossRef](#)]
21. Gamma Technologies | The Standard in Multi-Physics System Simulation. Available online: <https://www.gtisoft.com/> (accessed on 30 October 2020).
22. MathWorks—Makers of MATLAB and Simulink—MATLAB and Simulink. Available online: <https://www.mathworks.com/> (accessed on 30 October 2020).
23. Tribioli, L.; Chiappini, D.; Vukotić, M.; Miljavec, D. Performance Evaluation of an Electric Vehicle with Multiple Electric Machines for Increased Overall Drive Train Efficiency. *SAE Tech. Pap.* **2019**. [[CrossRef](#)]
24. Zheng, J.; Zhao, W.; Lee, C.H.T.; Ji, J.; Xu, G. Improvement torque performances of interior permanent-magnet machines. *CES Trans. Electr. Mach. Syst.* **2019**, *3*, 12–18. [[CrossRef](#)]
25. Rizzoni, G.; Guzzella, L.; Baumann, B.M. Unified modeling of hybrid electric vehicle drivetrains. *IEEE/ASME Trans. Mechatron.* **1999**, *4*, 246–257. [[CrossRef](#)]
26. Lee, S.; Cherry, J.; Safoutin, M.; McDonald, J.; Olechwi, M. Modeling and Validation of 48V Mild Hybrid Lithium-Ion Battery Pack. *SAE Int J. Altern. Powertrains* **2018**, *7*. [[CrossRef](#)]
27. REFPROP | NIST. Available online: <https://www.nist.gov/srd/refprop> (accessed on 30 October 2020).